



Infiltration of ionic-, electronic- and mixed-conducting nano particles into $\text{La}_{0.75}\text{Sr}_{0.25}\text{MnO}_3\text{--Y}_{0.16}\text{Zr}_{0.84}\text{O}_2$ cathodes – A comparative study of performance enhancement and stability at different temperatures

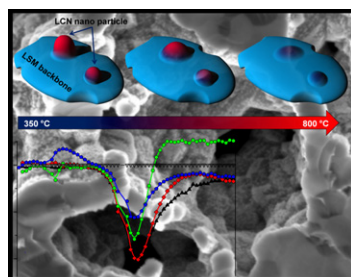
Ragnar Kiebach*, Christina Knöfel, Francesco Bozza, Trine Klemensø, Christodoulos Chatzichristodoulou

Department of Energy Conversion and Storage, Technical University of Denmark, Risø Campus, Frederiksborgvej 399, DK-4000 Roskilde, Denmark

HIGHLIGHTS

- In situ formation of nano particles leads to performance increase.
- Polarization resistance R_p decreased by more than 70%.
- The performance increase strongly differs with temperature and type of infiltrate.
- Mechanism of the performance increase independent from electrochemical properties.

GRAPHICAL ABSTRACT



ARTICLE INFO

Article history:

Received 5 October 2012

Received in revised form

16 November 2012

Accepted 20 November 2012

Available online 27 November 2012

Keywords:

Solid oxide fuel cell

LSM cathode

Infiltration

Impregnation

Nano particle

ABSTRACT

The microstructure and electrochemical performance of LSM–YSZ composite electrodes infiltrated with $\text{La}_{0.8}\text{Sr}_{0.2}\text{MnO}_{3-\delta}$ (LSM) as an electronic conductor, $\text{LaCo}_{0.6}\text{Ni}_{0.4}\text{O}_{3-\delta}$ (LCN) as a mixed conductor and $\text{Ce}_{0.8}\text{Gd}_{0.2}\text{O}_{2-\delta}$ (CGO) as an ionic conductor, were compared in the temperature range 550–800 °C. All three infiltrates resulted in improved electrochemical performance. Impedance analysis suggested dissociative adsorption and transfer of species to the triple phase boundary as the main mechanism responsible for the performance enhancement in all cases, attributed to the increase in surface area and triple phase boundary upon infiltration. LCN showed the most pronounced improvement at 550 °C, but its performance degraded drastically with increasing temperature. LSM and CGO infiltrated electrodes degraded less upon heating up to 800 °C. Infiltrated CGO electrodes showed the smallest degradation rate upon long term testing at 750 °C.

© 2012 Elsevier B.V. All rights reserved.

1. Introduction

Solid oxide fuel cells (SOFCs) are electrochemical devices that produce electricity directly from various fuels e.g. hydrogen, bio-ethanol or hydrocarbons [1–3]. Compared to traditional technologies, SOFCs exhibit high energy conversion efficiency, low noise level and reduced CO_2 emissions. Furthermore, the excellent load

following capability makes it ideal for playing an important role in future decentralized, intelligent power grids, if current challenges of high price, limited life time and insufficient performance are overcome.

State-of-the-art SOFCs typically utilise yttria stabilized zirconia (YSZ) as electrolyte and a Ni-YSZ cermet anode [4]. The most commonly used cathode material is a composite of YSZ and strontium doped lanthanum manganite ($\text{La}_{1-x}\text{Sr}_x\text{MnO}_{3-\delta}$ (LSM)) [5]. The operating temperature is in the range 800–1000 °C. Reduction of the operating temperature range to 550–750 °C (intermediate temperature (IT)) is currently a topic of much

* Corresponding author. Tel.: +45 46775624; fax: +45 46775688.

E-mail address: woki@dtu.dk (R. Kiebach).

research and development. IT-SOFCs can be economically favorable, as thermally activated degradation phenomena are minimized at lower temperatures, thereby increasing the life time. Furthermore, reducing the operating temperature allows the use of cheap materials for auxiliary components [6,7].

However, reduction of the operating temperature increases the ohmic and electrode polarization losses, the relative contribution of the cathode becoming the most significant due to its larger activation energy. Mixed ionic and electronic conducting (MIEC) materials, such as LSCF ($\text{La}_x\text{Sr}_{1-x}\text{Co}_y\text{Fe}_{1-y}\text{O}_3$), LCN ($\text{LaCo}_{0.6}\text{Ni}_{0.4}\text{O}_3$) and LSC ($\text{La}_x\text{Sr}_{1-x}\text{CoO}_3$) [8,9] are considered as cathodes for IT-SOFCs, due to their superior performance in comparison to LSM, but require a costly barrier layer (usually CGO) between the YSZ electrolyte and the cathode layers to prevent formation of electrical insulating secondary phases. A promising alternative is to improve the state-of-the-art and thermodynamically more stable LSM–YSZ cathode by introduction of (electro) catalytically active nano-materials into the porous cathode structure.

A way to obtain such nano-structured cathodes is the so called infiltration or impregnation process [10–23]. Here, nano particles are deposited into a pre-sintered backbone via an aqueous solution of metal salts. Low firing temperatures between 500 and 750 °C (compared to more than 1100 °C for sintering a LSM–YSZ composite) are sufficient to (in-situ) form and deposit the nano particles. These low firing temperatures have the advantage that a) the high catalytic activity and large triple phase boundary (TPB) areas, typical for nano sized particles, persist and b) that e.g. reaction between the MIEC material and the electrolyte, with the formation of electrical insulating secondary phases, can be minimized.

The infiltration of different materials into LSM–YSZ backbone structures has been reported in the literature [10–12,14–16,20,21] and an improved performance has been demonstrated for several materials. In these articles the main research focus is on finding the optimum particle loading to maximize the performance gain, and often highly concentrated solutions and/or a large number of repeated infiltration cycles are used to obtain a high density of particles along with an improved performance. However, studies comparing the effect of nano particles with different electrochemical properties on the performance, which could help determine the reaction mechanism, are still missing.

The aim of the present study is to contribute to fill this gap. Here, we compare how the performance of a standard LSM–YSZ composite electrode is influenced by the addition of three infiltrates with mainly different electrical conduction properties: a) $\text{La}_{0.8}\text{Sr}_{0.2}\text{MnO}_{3-\delta}$ (LSM) as an electronic conductor; b) $\text{LaCo}_{0.6}\text{Ni}_{0.4}\text{O}_{3-\delta}$ (LCN) as a mixed conductor and c) $\text{Ce}_{0.8}\text{Gd}_{0.2}\text{O}_{2-\delta}$ (CGO) as an ionic conductor. All materials were infiltrated via nitrate precursor solution into the LSM–YSZ backbone. The used infiltration process, temperature treatments and electrochemical test protocols were identical to allow comparison. Solutions with a relative low concentration of 0.3 M were used to favor the formation of isolated nano particles, which is useful for such fundamental studies. Additionally, a 3 M CGO solution was included in the test matrix to evaluate concentration effects of an ionic conductor. The changes in the microstructure and the electrochemical performance of the impregnated half cells were investigated in the temperature range from 550 °C to 800 °C. Impedance analysis was used to characterize losses and assign changes of the cell components and the electrochemical processes.

2. Experimental

Approximately 200 μm thick 8YSZ tapes ($\sim 4\text{ cm} \times 4\text{ cm}$) which have been prepared “in house” were used as electrolyte

layer. On both sides of these tapes, an ink consisting of 50/50 wt.% of $\text{La}_{0.75}\text{Sr}_{0.25}\text{Mn}_{1.05}\text{O}_{3\pm\delta}$ (LSM25) and $\text{Y}_{0.16}\text{Zr}_{0.84}\text{O}_{1.92}$ (8YSZ) was screen printed. After sintering above 1000 °C, the tapes were cut into small pieces of about $6 \times 6\text{ mm}$. The latter were used for the impregnation with nano particles and represent the not-impregnated reference materials [14]. The following solutions were used for infiltration: $\text{La}_{0.8}\text{Sr}_{0.2}\text{MnO}_3$ (LSM) (0.3 M), $\text{LaCo}_{0.6}\text{Ni}_{0.4}\text{O}_3$ (LCN) (0.3 M) $\text{Ce}_{0.8}\text{Gd}_{0.2}\text{O}_2$ (CGO) (3 M and 0.3 M). In each case an aqueous solution containing the metal nitrates in the appropriate ratio and the surfactant Pluoronic® P123 (BASF Cooperation) (0.5 mg ml^{-1}) was prepared. The following nitrates were used: $\text{La}(\text{NO}_3)_3 \cdot 6\text{H}_2\text{O}$ (Alfa Aesar, 99.9%), $\text{Sr}(\text{NO}_3)_2$ (Alfa Aesar, 99%), $\text{Mn}(\text{NO}_3)_2 \cdot 4\text{H}_2\text{O}$ (Alfa Aesar, 98%), $\text{Ni}(\text{NO}_3)_2 \cdot 4\text{H}_2\text{O}$ (Sigma Aldrich 98.5%), $\text{Co}(\text{NO}_3)_2 \cdot 6\text{H}_2\text{O}$ (Sigma Aldrich 98%), $\text{Gd}(\text{NO}_3)_3 \cdot 6\text{H}_2\text{O}$ (Sigma Aldrich 99.9%) and $\text{Ce}(\text{NO}_3)_3 \cdot 6\text{H}_2\text{O}$ (Sigma Aldrich 99.9%). The nitrate solution was then dropped onto the LSM–YSZ cathode and infiltrated into the pores by capillary forces. Afterward the samples were placed under vacuum to remove air pockets and enhance the penetration of the solution into the backbone, ensuring an even particle distribution throughout the complete porous electrode. The impregnated samples were dried at 350 °C before being used for electrochemical impedance spectroscopy (EIS) measurements. Prior to the EIS measurements, Pt paste was applied onto the symmetrical cells. Each cell was placed between Pt-grids connected to the electrochemical measurement equipment. The sample holder is placed in a furnace and EIS measurements were performed in compressed air flow. Two different temperature profiles were applied during EIS measurements: (a) EIS spectra were recorded at different temperatures starting from 550 °C with increasing the temperature in steps of 50 °C. The maximum temperature was 800 °C. After that, impedance spectra were recorded every 50 °C during cooling down to 550 °C. A last EIS measurement was performed at 750 °C. The various temperatures were kept constant for 2 h before the data collection. (b) Electrochemical impedance spectra were recorded at a constant temperature of 750 °C over approximately one week to determine electrochemical performance of the impregnated cells as a function of time. For the impedance measurements a Hioki frequency response analyzer was used. Open circuit conditions (OCV) were applied, using a 50 mV amplitude AC signal over a frequency range of 0.08 Hz–100 kHz with 10 points per decade. The impedance spectra were corrected for the inductance originating from the equipment such as wires etc. and normalized with the area of the symmetrical cells. 2–4 samples were made with each infiltrate to assure reproducibility. Polarization resistance values presented and discussed here are average values. The spread of these resistance values was below 15% for the impregnated cells showing a good reproducibility. Impedance data were analyzed using ZSimpWin 3.21, a program commercially available from EChem Software and applying the equivalent circuit $L R_s(RQ)(RQ)$ in Boukamp notation. For clarity and easier comparison the data in the Nyquist plots are presented after subtraction of the serial resistance (R_s).

Micrographs of the symmetrical cells and EDS spectra were recorded on a Zeiss Supra 35 scanning electron microscope (SEM) equipped with a field emission gun and an EDS detector.

3. Results and discussion

3.1. Microstructure of infiltrated LSM–YSZ (SEM/EDS)

To investigate temperature induced structural changes, SEM images from infiltrated samples annealed at 350, 550 and 750 °C (Fig. 1a–i) were compared. In all four infiltrated samples the in-situ formed nano particles are clearly observable in the SEM images for

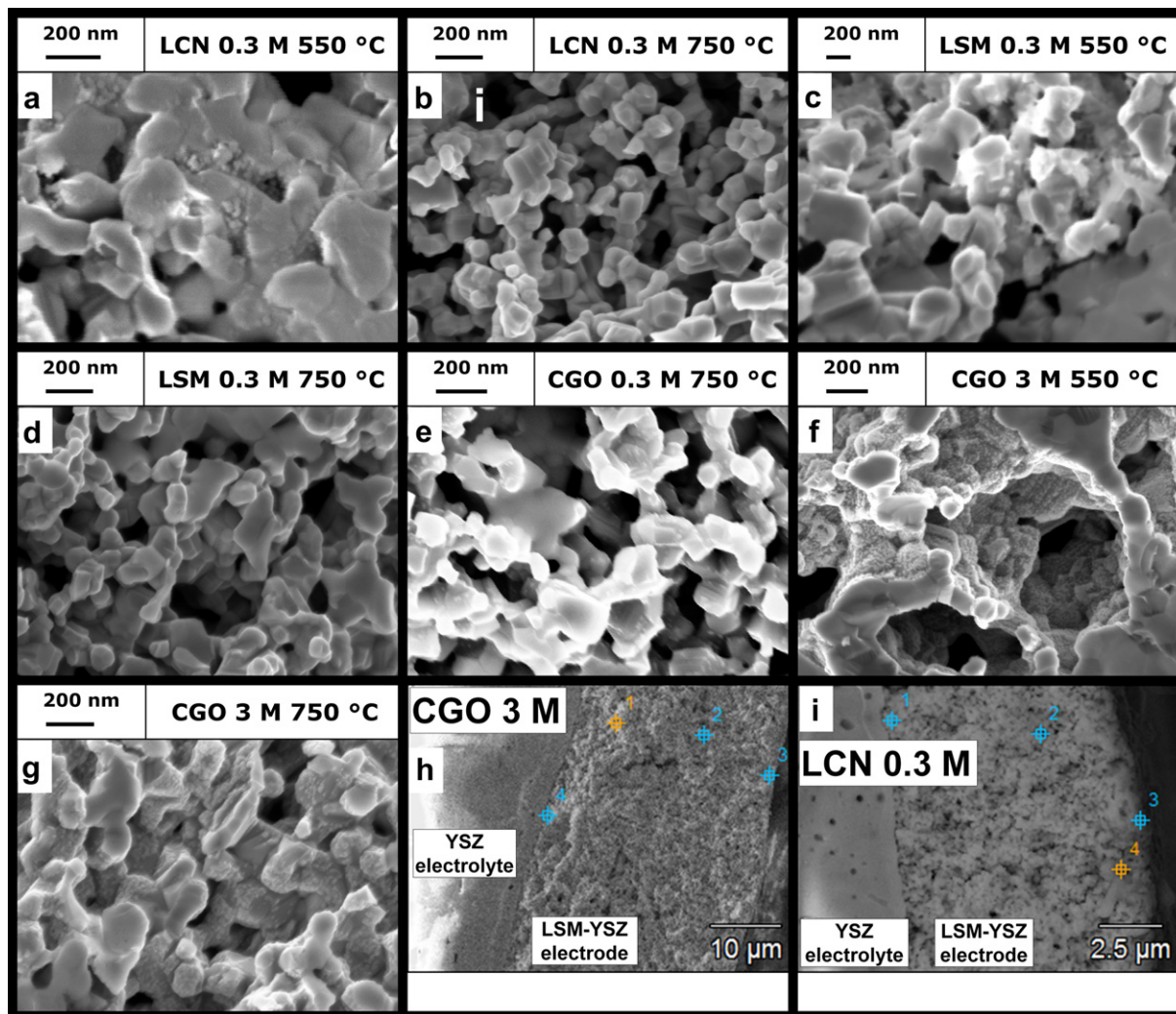


Fig. 1. Micrographs of fractured surfaces. a) LCN 0.3 M sintered at 550 °C, b) LCN 0.3 M sintered at 750 °C, c) LSM 0.3 M sintered at 550 °C, d) LSM 0.3 M sintered at 750 °C, e) CGO 0.3 M sintered at 750 °C, f) CGO 3 M sintered at 550 °C, g) CGO 3 M sintered at 750 °C, h) overview image of EDX analysis of CGO 3 M, i) overview image of EDX analysis of LCN 0.3 M.

the samples annealed at 350 °C (not depicted) and 550 °C (Fig. 1a, c and f). Each experiment was carried out three times to ensure reproducibility. In all cases particle size, shape and distribution are similar, indicating that the used infiltration process leads to well reproducible results. As expected, the density of the CGO particles when the 3 M solution (Fig. 1f and g) was used is significantly higher compared to the ones infiltrated with 0.3 M solutions (Fig. 1e). In the case of LSM and LCN, the infiltrated particles are not distributed completely even on top of the backbone particles. As indicated in Fig. 1a and c, the nano particles can occur in clusters with a large number of isolated particles, while in other areas only a few nano particles are found. The size of the particles can be estimated from 20 nm to 70 nm. For LSM and LCN impregnated samples annealed at 750 °C, no nano particles were found (Fig. 1b and d). It is well documented [18,19,21] that nano particles in clusters tend to sinter at this temperature, which leads to particle coarsening or agglomeration. In principle also for isolated nano particles the formation of larger particles through surface migration on the backbone particles could be possible, but no indications for such an agglomeration mechanism were found in the SEM images. Instead, it can be assumed that the nano particles sinter with or dissolve in the backbone structure in order to minimize their surface energy as illustrated in Fig. 2. For the CGO nano

particles this phenomena is not observed. Well dispersed CGO nano particles are found also in samples annealed at 750 °C.

Even though the total amount of infiltrated particles is relatively low, the presence and a regular distribution of infiltrated LCN and CGO could be verified by EDS analysis (Fig. 1h,i and Table 1). For samples infiltrated with 0.3 M LCN (Fig. 1h) the concentration of Co and Ni found are low, but still the amount of Co and Ni is high enough to be detected outside the error range by EDS. As expected, for samples infiltrated with 3 M CGO, Ce and Gd were found in significant amount at all investigated places (Fig. 1i). Since the

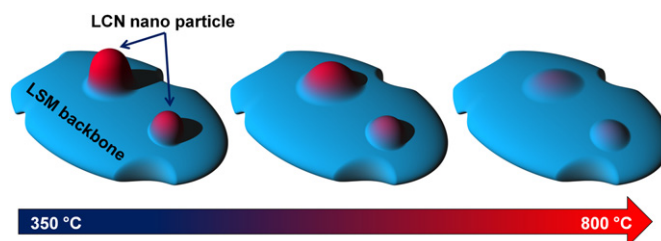


Fig. 2. Possible reaction mechanism of LCN nano particles with backbone structure at different temperatures.

Table 1

EDS composition analysis (at. %, error given in parentheses) for 3 M CGO and 0.3 M LCN. Elements introduced by infiltration marked in bold.

LCN 0.3 M							
	La	Sr	Mn	Zr	Y	Co	Ni
Point1	0.29 (0.1)	—	0.43 (0.1)	83.07 (0.5)	15.66 (0.5)	0.29 (0.2)	0.27 (0.2)
Point2	18.14 (0.3)	1.40 (0.1)	19.76 (0.4)	49.02 (0.3)	10.37 (0.2)	0.58 (0.2)	0.72 (0.2)
Point3	41.29 (0.3)	3.95 (0.1)	47.30 (0.5)	5.69 (0.2)	1.12 (0.2)	0.27 (0.2)	0.38 (0.2)
Point4	25.88 (0.2)	6.66 (0.1)	31.59 (0.4)	29.18 (0.3)	5.18 (0.2)	0.45 (0.2)	1.06 (0.2)
CGO 3 M							
	La	Sr	Mn	Zr	Y	Ce	Gd
Point 1	14.21 (0.6)	1.92 (0.3)	17.46 (0.7)	51.28 (0.9)	11.63 (0.8)	2.89 (0.4)	0.60 (0.3)
Point 2	28.23 (0.7)	6.95 (0.3)	35.72 (0.7)	17.14 (0.3)	3.95 (0.3)	6.96 (0.7)	1.05 (0.3)
Point 3	23.75 (0.6)	7.18 (0.3)	30.31 (0.7)	25.01 (0.4)	3.90 (0.4)	7.99 (0.4)	1.85 (0.3)
Point 4	0.98 (0.2)	—	1.02 (0.3)	82.66 (0.9)	13.93 (0.8)	1.18 (0.2)	0.23 (0.3)

elemental composition of the backbone and the infiltrate are similar in the case of the LSM infiltration, EDS measurements were not performed.

3.2. Electrochemical performance

3.2.1. Electrical performance at different temperatures

EIS spectra were recorded at each temperature in the following sequence of temperatures 550–600–650–700–750–800–750–700–650–600–550–750 °C. The temperature profile is also shown in Fig. 3, along with the decrease of the polarization resistance R_p values of the impregnated samples in comparison to the non-infiltrated samples at the different temperatures. Complementary, the R_p values for the various samples at the different temperatures are listed in Table 2. As represented in Fig. 3, the decrease of the R_p for the different infiltration solutions varies strongly with temperature. For LCN a strong decrease in R_p (up to 80%) is found, especially for the initial low temperature region below 600 °C in the heating up section of the experiment. In general, the benefit of infiltrating with LCN decreases with increasing temperature. At 800 °C the decrease of R_p found for LCN infiltrated samples is only 13%, which is the lowest of the tested

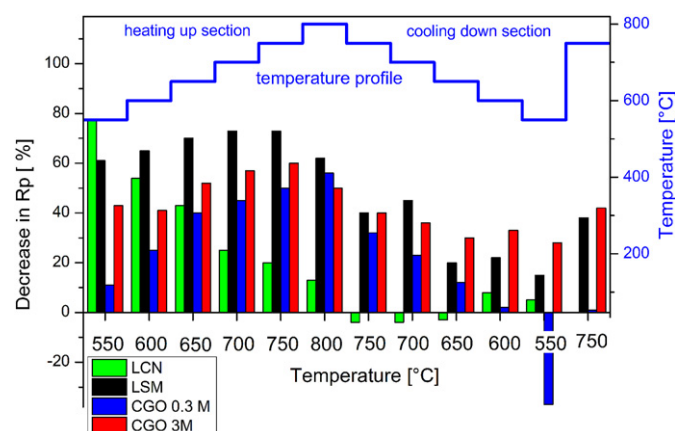


Fig. 3. Decrease of R_p of various infiltrated samples values relative to reference cell at different temperatures.

infiltration solutions. In the cooling down section LCN infiltrated cells did not show an improved performance, the R_p values found are comparable or even slightly higher than for the un-infiltrated reference samples. For LSM a relatively constant beneficial effect on the R_p is found for the whole temperature range. As a trend, a slight R_p decrease with increasing temperature is found, which is contrary to the LCN samples. In the heating up section the R_p decreases by 60–70% relative to the reference value for non-infiltrated LSM–YSZ. After reaching 800 °C, the performance improvement observed for LSM infiltrated cells in the heating up section is partly lost. Especially for the low temperature region between 650 and 550 °C the benefits of infiltration decreased (from 60% to 20%). The trend found for the CGO impregnated samples in the heating up section of the temperature profile in Fig. 3 is similar to that found for LSM. With increasing temperature the electrical performance of the infiltrated cells improves compared to the reference cell. The largest improvement for the CGO infiltrated cells is found above 700 °C, with the decrease in R_p at 800 °C being more than 50%.

As expected, the concentration of the CGO solution used for infiltration has an influence on the electrochemical performance. Cells infiltrated with 0.3 M CGO and 3 M CGO differ in the following three main points: a) the electrochemical performance of the cells infiltrated with the higher concentration is generally better (except at 800 °C); b) cells infiltrated with 3 M CGO performed significantly better at temperatures below 700 °C than cells infiltrated with 0.3 M CGO; c) cells infiltrated with 3 M CGO maintain the improved electrochemical performance after the high temperature treatment to a larger degree than the cells infiltrated with 0.3 M CGO.

In Fig. 4(top) the Nyquist plots are presented for chosen electrodes at 600 °C in the heating up section and the effect of the infiltration is clearly observable in the presented spectra.

The impedance of the LSM–YSZ composite cathode has been reported to consist mainly of two suppressed arcs in the temperature range 750–900 °C with characteristic summit frequencies of approximately 25 kHz and 200 Hz, respectively, at 750 °C [24–27]. The high frequency impedance arc of the cathode is reported to have a weak or no dependency on the oxygen partial pressure, and is ascribed to the transfer of oxygen intermediates/oxide ions between the LSM and the YSZ phase. In contrast, the low frequency impedance arc of the cathode is reported to have a strong dependency on the oxygen partial pressure, and is assumed to be associated with dissociative adsorption and transfer of species to the TPB. Reaction between the two phases of the LSM–YSZ composite is well known, and results in low conductive zirconates at the LSM–YSZ interface [28], which is expected to affect the high frequency arc [5,26,29]. However, systematic impedance studies over a very broad temperature range 400–900 °C have revealed the impedance to be more complicated than two suppressed arcs, which in particular becomes evident at temperatures lower than 700 °C [30].

A way to visualize which frequency domains are affected by a parameter change is the so-called analysis of differences in impedance spectra (ADIS). By knowing at which frequency domain different processes appear it may be possible to pinpoint which process is affected by a parameter variation or degradation during operation [31–33]. In the given context ADIS is used for studying the impact of infiltration. In Fig. 4, the ADIS plots for the different infiltrated cells at 600 °C in the heating up section (Fig. 4, middle) and 750 °C in the cooling down section (Fig. 4, bottom) are plotted.

At 750 °C, the ADIS spectrum (Fig. 4, bottom) shows that the impedance for all electrodes is mainly affected at frequencies between 50 and 500 Hz as a result of infiltration. This indicates [5,24–26,30,35] that it is the processes of dissociative adsorption and transfer of species to the TPB, that are affected by infiltration. However, a closer inspection reveals that for the LCN infiltrated

Table 2
Average polarization resistance R_p [$\Omega \text{ cm}^2$] and decrease of the R_p [%] compared to the reference cell at different temperatures for the various electrodes. Lowest R_p for each temperature marked in bold.

T [$^{\circ}\text{C}$]	Reference cell R_p [$\Omega \text{ cm}^2$]	LCN R_p [$\Omega \text{ cm}^2$]	Decrease in R_p [%]	LSM R_p [$\Omega \text{ cm}^2$]	Decrease in R_p [%]	CGO 0.3 M R_p [$\Omega \text{ cm}^2$]	Decrease in R_p [%]	CGO 3M R_p [$\Omega \text{ cm}^2$]	Decrease in R_p [%]
550	4.34	0.99	77	1.7	61	3.88	11	2.49	43
600	1.65	0.75	54	0.57	65	1.23	25	0.97	41
650	0.94	0.54	43	0.28	70	0.56	40	0.45	52
700	0.51	0.38	25	0.14	73	0.28	45	0.22	57
750	0.3	0.24	20	0.08	73	0.15	50	0.12	60
800	0.16	0.14	13	0.06	62	0.07	56	0.08	50
750	0.25	0.26	−4	0.15	40	0.17	32	0.15	40
700	0.47	0.49	−4	0.34	45	0.36	23	0.3	36
650	0.92	0.95	−3	0.74	20	0.81	12	0.64	30
600	2.08	1.91	8	1.63	22	2.03	2	1.39	33
550	5.08	4.81	5	4.32	15	6.96	−37	3.65	28
750	0.26	0.26	0	0.16	38	0.26	1	0.15	42

electrodes it is not only the low frequency part which changes. From Fig. 4 bottom, it is possible to see that the impedance of the low frequency part is lowered while the impedance of the high frequency part is increased. These observations are in accordance with the general knowledge that the LCN perovskite is less thermodynamically stable than LSM e.g. due to the introduction of more defects into the perovskite structure [9,31]. This makes the LCN phase more reactive with YSZ than LSM with the result of an increased formation of zirconates such as $\text{La}_2\text{Zr}_2\text{O}_7$. Thus, LCN infiltration improves the reduction of oxygen but the charge transfer of oxide ion species from LCN infiltrated LSM particles to the cathode YSZ ionic network or YSZ electrolyte is worsened due to the formation of insulating $\text{La}_2\text{Zr}_2\text{O}_7$ at the LSM–LCN–YSZ TPB. For the other types of infiltrates no increase in the transfer of oxide ion species is observed, as expected, since insulating solid state reaction products are not formed.

At 600 $^{\circ}\text{C}$ (Fig. 4, middle), similar observations can be made from the ADIS spectra of LCN, LSM and CGO; but a shift to lower frequencies is observed, which correlates well with increasing polarization resistances [5,24–26,30,35] but approximately constant capacitances at the decreased temperature. In the high frequency region as well as in the low frequency region below a few Hz no changes in the impedances caused by infiltration were found at 600 $^{\circ}\text{C}$.

3.2.2. Degradation caused by high temperature treatment

The decrease in R_p at 600 $^{\circ}\text{C}$, before and after reaching the maximum temperature of 800 $^{\circ}\text{C}$, is plotted in Fig. 5. It is clear that the various samples are influenced in a different way by the exposure at 800 $^{\circ}\text{C}$. For LCN and 0.3 M CGO the original improvement in the electrochemical performance is almost entirely lost. The degradation in samples infiltrated with 0.3 M LSM is much lower. Samples infiltrated with 3 M CGO showed only minor degradation after exposure to the temperature of 800 $^{\circ}\text{C}$. Despite the significant degradation of the LSM infiltrated cells (66%) after heat treatment at 800 $^{\circ}\text{C}$, the R_p is still 23% lower compared to the reference cell. Long-term aging effects must also be taken into consideration though, as discussed in Section 3.2.3 below.

3.2.3. Long-term degradation at constant temperature

To investigate the long-term stability of the infiltrated cells, the electrochemical performance of the various infiltrated electrodes was recorded at a constant temperature of 750 $^{\circ}\text{C}$ for 150 h. The corresponding R_p values over time are shown in Fig. 6. As expected, the R_p values for the infiltrated cells at the start of the experiment are significantly lower than that of the reference cell and correspond well with the results of Section 3.2.1.

While the reference cells show a linear degradation behavior over the entire time period, the infiltrated cells show a different behavior, especially in the first 50 h of the experiment. After 50 h, the degradation of all infiltrated electrodes can be described as linear. The R_p values at the beginning of the experiment and 50 h later are presented in Table 3. Based on these data, the absolute and relative degradation for the first 50 h are calculated (Table 3). From the infiltrated samples, the 3 M CGO infiltrated cell showed the lowest relative degradation (15%/100 h), followed by the LCN (20%/100 h) and 0.3 M CGO (22%/100 h). The sample infiltrated with LSM had by far the highest degradation rate with 70%/100 h, indicating that most benefits of the infiltration are already lost after the first 50 h. To evaluate the long-term stability of the infiltrated cells, the degradation rates were determined for the last 100 h of the experiment (between 50 h and 150 h). The results are summarized in Table 3.

The electrodes infiltrated with LCN and 0.3 M CGO show a similar degradation profile as the reference. For both solutions, the relative degradation rates are similar or a little lower (LCN 6.8%/100 h; 0.3 M CGO 6.0%/100 h) compared to the un-infiltrated reference cell (7.2%/100 h). Higher degradation rates were found for LSM (31.6%/100 h) and 3 M CGO (23.4%/100 h), indicating that the use of these materials, despite their good initial performance, could be problematic on the long term. All samples showed linear degradation behavior after 150 h. Therefore experiments were stopped since no more valuable information would be obtained. It has to be mentioned, that the degradation rates of the symmetrical cells are higher compared to normal SOFC cells. The reason therefore is a weaker contact of the current collector (Pt) with the symmetrical cell, due to a relative low sintering temperature. Higher sintering temperatures would lead to a better contact and lower degradation rates, but also to a reaction of the infiltrated nano particles with the backbone structure before the actual measurements, making a study of the temperatures dependence impossible. Therefore the sintering temperature of the Pt contact was kept below the actual test temperatures, compromising the long term stability to a certain degree.

Also for this study at constant temperature the ADIS method was applied to obtain further insight in the degradation mechanism. In Fig. 7a, representative ADIS plots for the reference cell and cells infiltrated with 0.3 M CGO and 3 M CGO are shown. The differences were calculated as a function of time and with respect to the first spectra at the beginning of the experiment. For all samples the ADIS spectra below 10 Hz show only insignificant values and these are therefore neglected. The reference cell shows an increase of impedance between 10 and 1000 Hz as a function of time (Fig. 7a top). No changes are detected at higher frequencies. This indicates that the gas solid interactions are changing with time

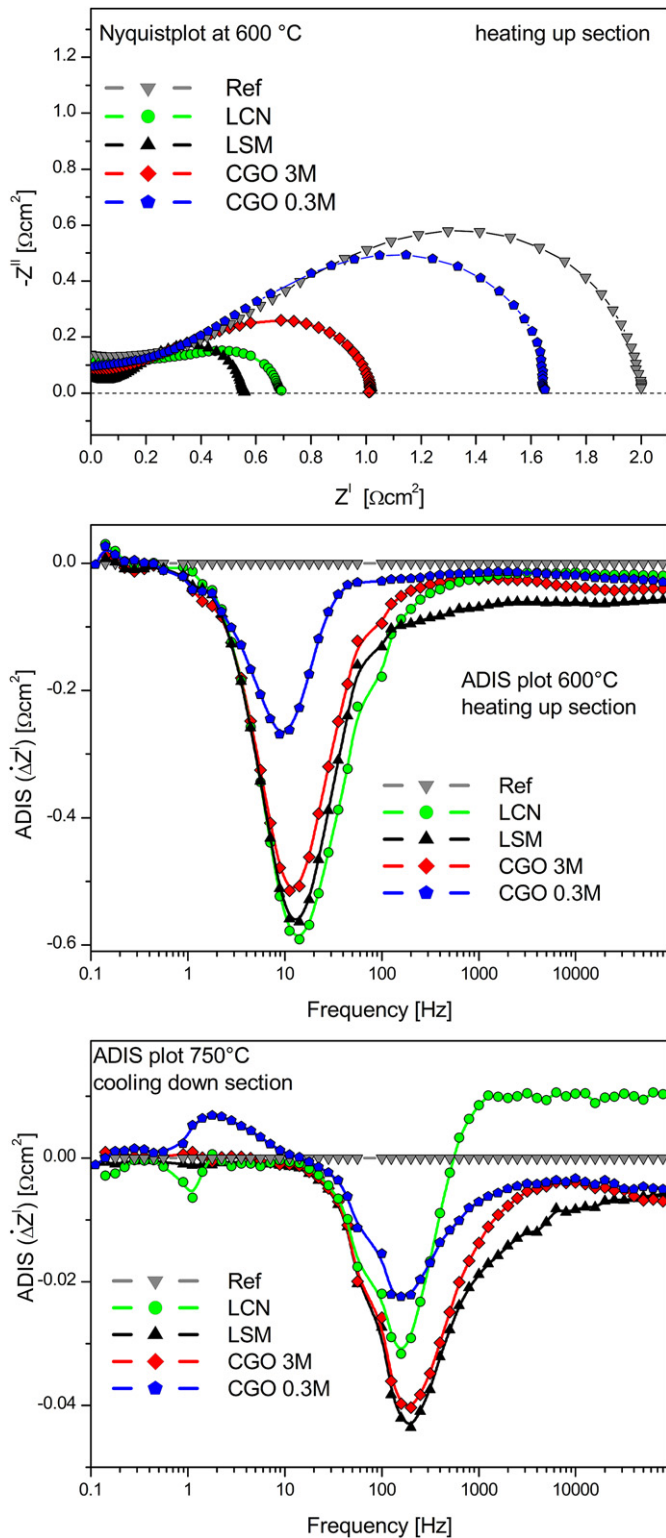


Fig. 4. Nyquist plot for different samples at 600 °C (top), ADIS plot for different samples at 600 °C (middle) and 750 °C (bottom).

while solid–solid interactions seem not to affect or contribute to the degradation in this case [5,24–26,30,35].

The infiltrated samples show a similar behavior, in all cases the most significant changes are found in the region between 10 and 1000 Hz (Fig. 7a middle, bottom). This is in accordance with the

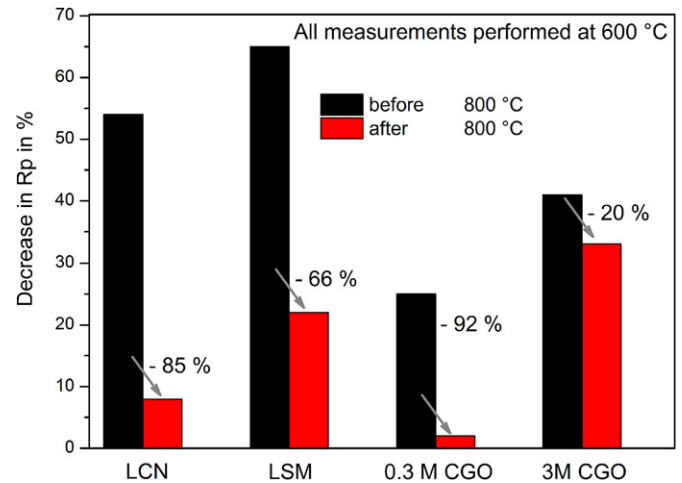


Fig. 5. Decrease in R_p before and after heat treatment at 800 °C for various samples.

data discussed in Section 3.2.1 and can be interpreted as a decrease of the surface area over time. Additionally, for samples infiltrated with 3 M CGO a small increase of the impedance in the high frequency range was found. This change in the shape of the spectra and an increase of the R_s over time become more obvious in the Nyquist plot for electrodes infiltrated with 3 M CGO (Fig. 7b) and is not observed for the samples infiltrated with 0.3 M solutions (data for 0.3 M CGO shown for comparison in Fig. 7b).

This high frequency response in Fig. 7b at the beginning of the experiment can be associated with the transfer of oxygen intermediates/oxide ions between the LSM and the YSZ phase, and the presence of low conductive zirconates at the interface. For infiltration with 3 M CGO, the concentration of CGO placed at the TPB is high enough to shunt the high frequency LSM–YSZ interfacial impedance response by providing an alternative conduction path. Instead of oxygen reduction at the LSM phase near the TPB combined with oxide ion transport through the LSM–YSZ interface, the oxygen reduction can also take place at the LSM/CGO followed by oxide ion transport through the infiltrated CGO into the YSZ. This would reduce the blocking effect of the zirconates at the interface, and be reflected in both the high frequency response and improved lower frequency response. A detailed discussion of this effect and the corresponding changes and analysis of the impedance spectra can be found here [34]. Over time, the benefit of the “bridging” CGO is lost, probably due to sintering and coarsening of the CGO particles.

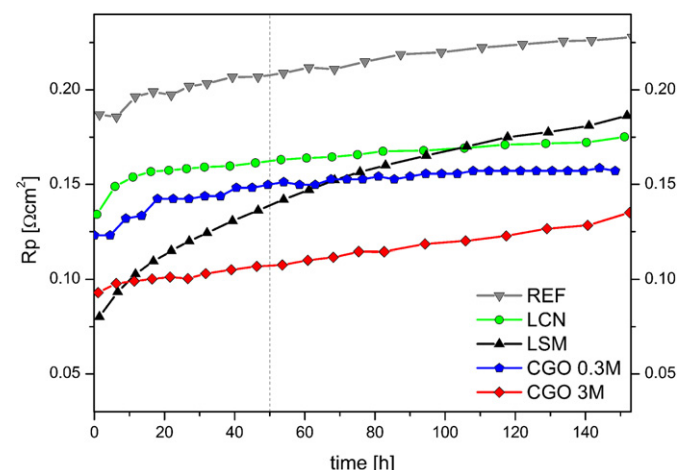


Fig. 6. Development of R_p at 750 °C as a function of time for the various samples.

Table 3
Results from long term testing.

	R_p start [$\Omega\text{ cm}^2$]	R_p after 50 h [$\Omega\text{ cm}^2$]	Degradation after 50 h [$\Omega\text{ cm}^2$]	Degradation after 50 h [%]	Degradation rate during 50–150 h [$\Omega\text{ cm}^2/100\text{ h}$]	Degradation rate during 50–150 h [%/100 h] (relative to R_p @ 50 h)
Ref	0.187	0.207	0.02	11	0.015	7.2
LCN	0.134	0.161	0.027	20	0.011	6.8
LSM	0.080	0.136	0.056	70	0.043	31.6
CGO 0.3 M	0.123	0.150	0.027	22	0.009	6.0
CGO 3 M	0.093	0.107	0.014	15	0.025	23.4

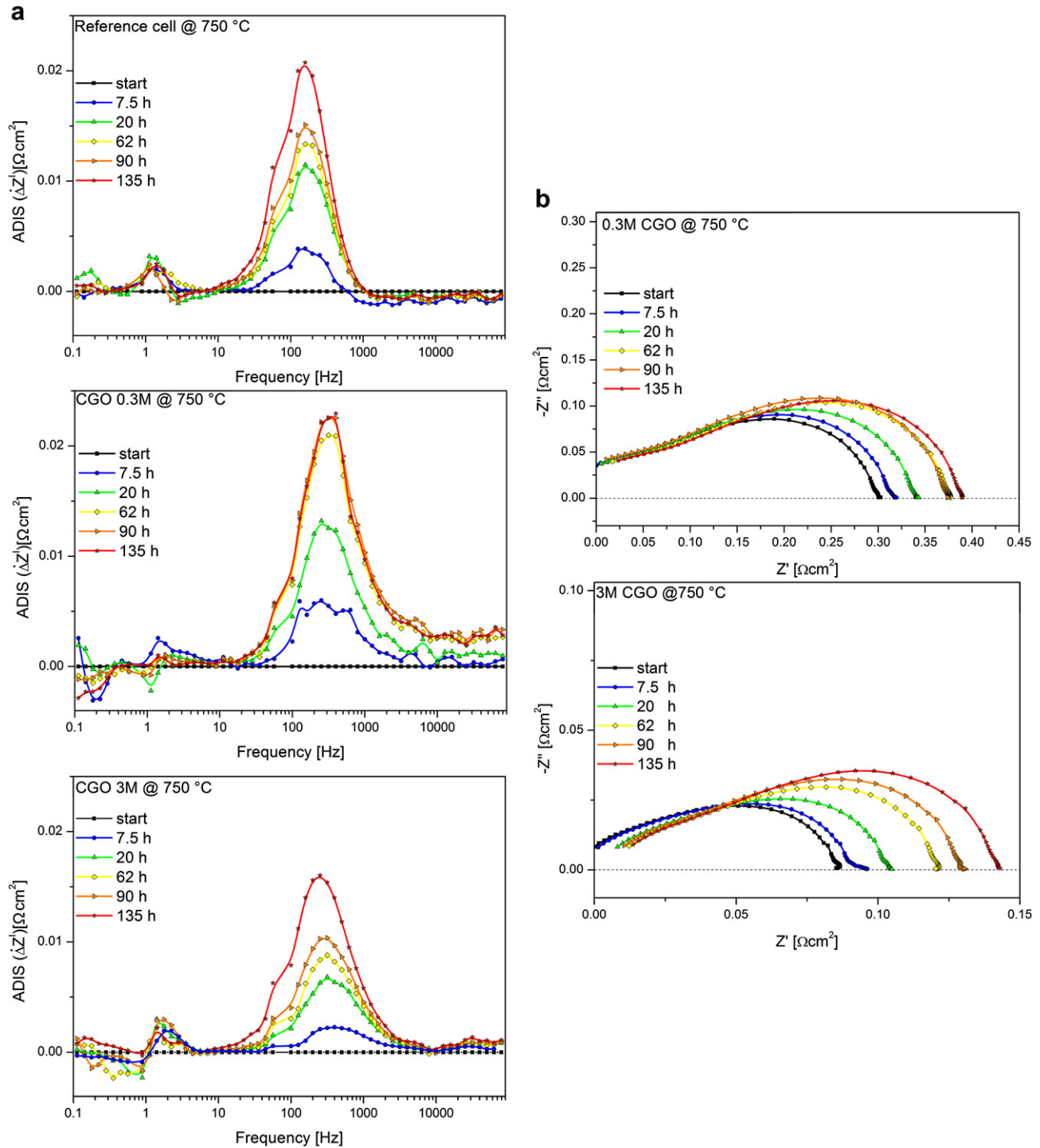


Fig. 7. a) ADIS plots for the reference cell (top), CGO 0.3 M (middle) and CGO 3 M (bottom) at 750 °C as a function of time. b) Nyquist plots for CGO 0.3 M (top) and CGO 3 M (bottom) at 750 °C as a function of time. The plot for 3 M CGO is shown in threefold magnification to facilitate comparison.

4. Conclusion

The results from impedance/ADIS analysis suggest that the main mechanism responsible for the performance enhancement is identical even if the degree of the effect on the electrochemical performance differs strongly between the tested infiltration solutions. Generally it can be assumed, that isolated nano clusters/agglomerates of the infiltrate are formed after infiltration, resulting in a large increase of the surface area. Especially nano particles close to the triple phase boundary increasing the length of the same are beneficial for the electrochemical performance. The electrical conduction properties (electronic conductor, ionic conductor or mix conductor) of the infiltrated materials seem to have minor or no influence on the reaction mechanism, but electronic conducting materials like LSM and LCN seems to be especially beneficial at lower temperatures. It is well known, that CGO, LCN and LSM are catalytically active for the oxygen reduction in air, but the role of the catalytic activity of the different materials seems less important. The stability of the enlarged surface area strongly differs with the type of infiltrate. While LCN and LSM seem to react with the backbone structure already at temperatures below 800 °C, infiltrated CGO particles are more stable. From a practical point of view, the use of LCN could be beneficial for applications at temperatures below 600 °C. Considering long term stability, infiltrated CGO seems to be the best choice since the degradation rate for this material is relatively low. The concentration of the used infiltration solutions in the here presented experiments was very low, and it can be expected that infiltration with higher concentration and more infiltration cycles may lead to even better performance.

Acknowledgment

This work was supported financially by the Department of Energy Conversion and Storage, Technical University of Denmark. The authors also thank the technical staff at the Department of Energy Conversion and Storage for technical support in sample fabrication and characterization.

References

- [1] S. Linderoth, A. Smith, *Ceram. Eng. Sci. Proc.* 28 (2008) 3–13.
- [2] R.M. Miller, T. Reitz, *Ceram. Eng. Sci. Proc.* 31 (2010) 1–14.
- [3] L. Blum, *Ceram. Forum Int.* 86 (2009) E17–E22.
- [4] N. Vivet, S. Chupin, E. Estrade, A. Richard, S. Bonnamy, D. Rochais, E. Bruneton, *J. Power Sources* 196 (2011) 9989–9997.
- [5] S.B. Adler, *Chem. Rev.* 104 (2004) 4791–4843.
- [6] M.C. Tucker, *J. Power Sources* 195 (2010) 4570–4582.
- [7] T. Klemensø, J. Nielsen, P. Blennow, Å.H. Persson, T. Stegk, B.H. Christensen, S. Sønderby, *J. Power Sources* 196 (2011) 9459–9466.
- [8] J.C.H. Rossiny, J. Julis, S. Fearn, J.A. Kilner, Y. Zhang, L. Chen, S. Yang, J.R.G. Evans, *Solid State Ionics* 179 (2008) 1085–1089.
- [9] P. Hjalmarsson, M. Søgaard, A. Hagen, M. Mogensen, *Solid State Ionics* 179 (2008) 636–646.
- [10] Z. Jiang, C. Xia, F. Chen, *Electrochim. Acta* 55 (2010) 3595–3605.
- [11] Z. Liu, D. Ding, B. Liu, W. Guo, W. Wang, C. Xia, *J. Power Sources* 196 (2011) 8561–8567.
- [12] M. Mogensen, M. Søgaard, P. Blennow, K.K. Hansen, 8th European SOFC Forum Lucerne, Lucerne Fuel Cell Forum, Switzerland, 2008, A0402.
- [13] F. Bidrawn, G. Kim, N. Aramrueang, J.M. Vohs, R.J. Gorte, *J. Power Sources* 195 (2010) 720–728.
- [14] P. Knöfel, H.-J. Wang, K.T.S. Thydén, M. Mogensen, *Solid State Ionics* 195 (2011) 36–42.
- [15] S.P. Jiang, *Mater. Sci. Eng. A* 418 (2006) 199–210.
- [16] S.P. Jiang, *Int. J. Hydrogen Energy* 37 (2012) 449–470.
- [17] T.Z. Sholklapper, C.P. Jacobson, S.J. Visco, L.C. De Jonghe, *Fuel Cells* 8 (2008) 303–312.
- [18] J.M. Vohs, R.J. Gorte, *Adv. Mater.* 21 (2009) 943–956.
- [19] J.S. Kim, S. Lee, R.J. Gorte, J.M. Vohs, *J. Electrochem. Soc.* 158 (2010) B79–B83.
- [20] K. Yamahara, C.P. Jacobson, S.J. Visco, L.C. De Jonghe, *Solid State Ionics* 176 (2005) 451–456.
- [21] M. Shah, P.W. Voorhees, S.A. Barnett, *Solid State Ionics* 187 (2011) 64–70.
- [22] Y. Huang, J.M. Vohs, R.J. Gorte, *J. Electrochem. Soc.* 153 (2006) A951–A955.
- [23] C. Lu, T.Z. Sholklapper, C.P. Jacobson, S.J. Visco, L.C. De Jonghe, *J. Electrochem. Soc.* 153 (2006) A1115.
- [24] M.J. Jørgensen, M. Mogensen, *J. Electrochem. Soc.* 148 (2001) A433–A442.
- [25] S.P. Jiang, *J. Mater. Sci.* 43 (2008) 6799–6833.
- [26] R. Barfod, M. Mogensen, T. Klemensø, A. Hagen, Y.L. Liu, P.V. Hendriksen, *J. Electrochem. Soc.* 154 (2007) B371.
- [27] J. Nielsen, M. Mogesen, *Solid State Ionics* 189 (2011) 74–81.
- [28] Y.L. Liu, A. Hagen, R. Barfod, M. Chen, H.J. Wang, F.W. Poulsen, P.V. Hendriksen, *Solid State Ionics* 180 (2009) 1298–1304.
- [29] C. Chatzichristodoulou, M. Chen, J.R. Bowen, Y.-L. Liu, Yi-Lin, *J. Am. Ceram. Soc.* 93 (2010) 2884–2890.
- [30] N. Bonanos, B.C.H. Steele, E.P. Butler, E. Barsoukov, J.R. McDonald (Eds.), *Impedance Spectroscopy – Theory, Experiment, and Application*, John Wiley & Sons Inc., Hoboken, NJ, 2005, pp. 258–263.
- [31] S.C. Grice, W.R. Flavell, A.G. Thomas, S. Warren, P.G. Marr, D.E. Jewitt, N. Khan, P.M. Dunwoody, S.A. Jones, *Surf. Rev. Lett.* 9 (2002) 277–283.
- [32] T. Ramos, J. Hjelm, M. Wandel, A. Hagen, M. Mogensen, *ECS Trans.* 13 (2008) 235–248.
- [33] S.H. Jensen, A. Hauch, P.V. Hendriksen, M. Mogensen, N. Bonanos, T. Jacobsen, *J. Electrochem. Soc.* 154 (2007) B1325–B1330.
- [34] T. Klemensø, C. Chatzichristodoulou, J. Nielsen, F. Bozza, K. Thydén, R. Kiebach, S. Ramousse, *Solid State Ionics* 224 (2012) 21–31.
- [35] N. Bonanos, P. Holtapples, M.J. Jørgensen, 5th European SOFC Forum Lucerne, Lucerne Fuel Cell Forum, Switzerland, 2002, 578–585.